

# Using Lidar Intensity for Robot Navigation

Adarsh Jagan Sathyamoorthy<sup>1\*</sup>, Kasun Weerakoon<sup>1\*</sup>, Mohamed Elnoor<sup>1</sup>,  
and Dinesh Manocha<sup>1</sup>.

**Abstract**—We present (Multi-Layer Intensity Map), a novel 3D object representation for robot perception and autonomous navigation. They consist of multiple stacked layers of 2D grid maps each derived from reflected point cloud intensities corresponding to a certain height interval. The different layers of the intensity maps can be used to simultaneously estimate obstacles’ height, solidity/density, and opacity. We demonstrate that they can help accurately differentiate obstacles that are safe to navigate through (e.g. beaded/string curtains, pliable tall grass), from ones that must be avoided (e.g. transparent surfaces such as glass walls, bushes, trees, etc.) in indoor and outdoor environments. Further, to handle narrow passages, and navigate through non-solid obstacles in dense environments, we propose an approach to adaptively inflate or enlarge the obstacles detected on intensity maps based on their solidity, and the robot’s preferred velocity direction. We demonstrate these improved navigation capabilities in real-world narrow, dense environments using a real Turtlebot and Boston Dynamics Spot. We observe significant increases in success rates (up to 50%), a 9.55% decrease in trajectory length, and up to a 10.9% increase in the F-score compared to current navigation methods using other sensor modalities.

## I. INTRODUCTION

Mobile robots have been used to navigate in indoor environments (such as households, offices, hospitals, etc. [1], [2], [3]), and outdoor environments such as agricultural fields, forests, etc. [4], [5], [6]. Such complex environments contain obstacles of various sizes, densities/solidities, and opacities that are challenging in terms of the robot’s perception, and navigation. For instance, contemporary indoor environments contain objects such as string/beaded curtains, transparent surfaces such as glass walls [7], [8], etc. Outdoor scenarios, on the other hand, have complex vegetation such as pliable tall grass, bushes, trees, etc. in close proximity to and intertwined with each other. A major challenge, and an important requirement for autonomous navigation, is differentiating *truly solid* and impassable obstacles (furniture, glass surfaces, bushes, trees, etc.) from obstacles that can be passed through (beaded curtains, tall grass, etc.).

To first detect obstacles, mobile robots have predominantly used RGB and depth images [9], 2D lidar scans [10], 3D point clouds [11], etc. The raw data from these sensors has been used to: (1). Estimating the proximity of objects in the robot’s vicinity, (2). Computing a variation of an occupancy grid [12] or a cost map representation that indicates both an obstacle’s size and distance from the robot, or (3). Segmenting the scene to assess obstacles’ size, distance, and semantic meaning [13], [14]. Although such approaches have



Fig. 1: Comparison of navigation trajectories generated using: Intensity maps (ours); DWA with laser scan [10]; DWA with occupancy map [12]; Spot’s Inbuilt Autonomy; and VERN [16] in complex vegetation. Intensity maps’s multi-layer intensity map formulation identify solid objects such as trees even when they are hidden behind navigable vegetation.

been used to aid navigation, they may not work well in environments composed of thin, pliable/bendable, and transparent obstacles. For instance, time-of-flight sensors such as depth cameras and lidars tend to detect thin, pliable, and passable obstacles (e.g. string curtains, tall grass) as solid obstacles that the robot must avoid [15]. On the other hand, transparent objects such as glass remain undetected since the laser rays mostly pass through them, leading to collisions during navigation. Similarly, perception methods using RGB images may not work well in terms of detecting transparent objects and visually similar but structurally dissimilar vegetation. Moreover, they are severely affected by the environment’s lighting changes.

**Main Contributions:** In order to address these robot perception challenges, we present a novel obstacle representation called Multi-layer Intensity Maps, a *multi-layer intensity map* that can be used to simultaneously estimate the size/height, density/solidity, and opacity of objects in the environment. They are constructed by stacking individual layers of 2D grid maps, each computed from reflected point clouds intensities corresponding to a certain height interval. It preserves the benefits of existing occupancy grids such as indicating the size and proximity of obstacles around the robot while also accurately detecting passable obstacles as such. The novel components of our approach include:

- A novel obstacle representation called the multi-layer intensity map constructed from the intensities of the reflected points in a point cloud. In addition to an

\* Authors contributed equally.

<sup>1</sup>Authors are with the University of Maryland, College Park.

object’s height and size, the multi-layer intensity map also reflects its true density/solidity. Our multi-layer intensity map can replace occupancy grids and other map representations in existing navigation methods to enable a robot to navigate through passable/navigable indoor and outdoor obstacles that are often misclassified by existing representations.

- A novel method to detect transparent objects using the low-intensity reflected points in the multi-layer intensity map. Our approach accurately extrapolates the transparent surfaces from a small neighborhood of low-intensity points which enables a robot’s motion planner to avoid collisions, significantly improving its rate of safely reaching its goal.
- A novel method using the multi-layer intensity map to accurately identify objects that are safe to navigate through such as thin, passable curtains in indoor scenarios, and pliable tall grass in outdoor environments. Our approach alleviates robot freezing behaviors in the presence of such objects.
- An adaptive inflation strategy that assesses the available free-space, and the detected solid obstacles (e.g. concrete and glass walls, furniture indoors, and bushes and trees outdoors) to enlarge them in the multi-layer intensity map for efficient planning. Our strategy handles narrow scenarios such as doors, corridors, and passages between dense vegetation and trees, where existing navigation schemes freeze.

## II. RELATED WORK

In this section, we give a brief overview of perception methods that use point cloud intensities. Additionally, we review the existing obstacle detection research in indoor and outdoor settings.

### A. Sensing using Point Cloud Intensity

The importance of intensity information in LiDAR point cloud data has been an emerging focus in robotics [17], [18], [19]. Some methods investigate the use of intensity information alongside geometric features to enhance point cloud classification methods in outdoor settings [20]. These methods highlight the potential of using the intensity information to provide a better understanding of obstacles, particularly when scene illumination is not consistent. Other methods include the ISHOT descriptor [21], which combines geometric and intensity data for improved place recognition. Lidar intensity maps have been also used for localization [22], [23], [24]. In [22], the authors present a robust Graph-SLAM framework that improves map accuracy for autonomous vehicles by encoding road surfaces based on LIDAR reflectivity. Moreover, the application of LiDAR intensity in visual navigation tasks has been explored. For instance, [25] introduces a lidar-intensity-image pipeline and demonstrates its performance in visual odometry (VO) and visual teach and repeat (VT&R) tasks. Lidar intensity maps have also been leveraged for various other applications,

including orthoimage generation [26] and anisotropic surface detection [27].

### B. Detecting Indoor Obstacles

Object detection in indoor settings has been widely studied for numerous applications including robot navigation, mapping, and computer graphics. Popular solutions in the literature include vision-based object detection and semantic segmentation approaches due to the structuredness of indoor environments. Moreover, the generation of necessary image datasets is feasible due to the limited diversity of indoor objects. However, detecting non-opaque objects such as glass remains a formidable challenge for vision-based systems due to the lack of visual clues. The method in [7] proposes GNet, a glass detection network that identifies abundant contextual cues for glass detection using a large-field contextual feature integration (LCFI) module. UCTNet [13] proposes a cross-modal transformer network for indoor RGB-D semantic segmentation to identify different objects such as curtains, doors, etc. However, such methods require large datasets with pixel-level ground truth labeling.

### C. Detecting Outdoor Obstacles

Over recent years, there has been significant progress in the development of robotic systems designed for outdoor navigation [28], [29], [30], [14], [31]. One early approach can be found at [32], where the usage of laser measurements enabled navigation capabilities for robots such as detecting short and grass-like vegetation. However, this method is not universally applicable, particularly in complex, unstructured vegetative terrains. Complementary approaches have tackled associated issues in off-road navigation, specifically concerning varying slopes [33] and different terrains [34].

Many studies integrate proprioceptive with exteroceptive sensory data to enhance outdoor navigation [35], [36], [37]. Machine learning techniques have also been incorporated to augment the robot’s capabilities for navigating through pliable vegetative obstacles [38], [39]. To this end, [16] uses a few shot learning approach to classify RGB vegetation images based on their traversability. This classifier is then integrated with a 3D LiDAR to construct a vegetation-aware traversability cost map.

## III. BACKGROUND

### A. Definitions and Assumptions

Our formulation assumes that a sensor capable of generating 3D point clouds (e.g., 3D lidar, depth camera) is mounted on a robot with a 2D linear ( $v$ ) and angular ( $\omega$ ) velocity space. Rigid coordinate frames are attached to the robot and sensor with the positive  $x, y, z$  directions facing forward, left, and upwards respectively, and for simplicity, we assume both frames to coincide. All positions, and velocities are measured relative to these frames. At any time  $t$ , the robot has a preferred velocity direction aimed at its goal  $(g_x, g_y)$  as  $\theta = \tan^{-1}(g_y/g_x)$ .

Our approach is based on using the reflected intensities of point clouds that could be obtained from sensors such as 3D

lidars, depth cameras, etc that have a laser source/transmitter and a receiver. We represent a point  $\mathbf{p}$  in a point cloud as  $\mathbf{p} = \{x, y, z, int\}$ , where  $x, y, z$  denote the point's location relative to the sensor, and  $int \in [0, R]$  denotes its intensity. We define a 2D robot-centric grid map as containing  $n \times n$  grids. Each grid is denoted by a row  $r$  and column  $c$ . Each grid represents a  $g \times g$  area in the real-world, and the value contained in it indicates the probability of the presence of an obstacle. Finally, we use  $j$  and  $k$  to denote indices.

### B. Point Cloud Intensity

Typically, a point's intensity is high ( $int > 0.75R$ ) when it is reflected from solid, opaque, 3D (length, width, and height dimensions are not infinitesimal) objects since they prevent the sensor's laser rays from passing through, or scattering away from the sensor. In contrast, objects that are low density (e.g. tall grass which is a collection of thin blades of grass that scatter laser rays), and transparent (e.g. glass where laser rays mostly pass through) lead to low intensities ( $int < 0.5R$ ) or in some cases, no intensity ( $int = 0$ ).

### C. Obstacle Properties

Our formulation leverages the property to accurately detect truly solid objects from the following categories defined based on how objects are sensed by existing perception modalities (2D lidar scan, RGB and depth images, etc) as:

- **True Positives (TP):** Solid, non-traversable objects detected as solid, e.g. walls, wooden furniture, humans, etc.
- **True Negatives (TN):** Non-solid, traversable objects detected as passable or no obstacle, e.g. free space.
- **False Positives (FP):** Non-solid objects detected as solid, e.g. string/beaded curtains, pliable tall grass.
- **False Negatives (FN):** Solid objects detected as non-solid or as free space, e.g. transparent objects.

### D. Obstacle Inflation

Once a truly solid object is detected, it must be enlarged or *inflated* for the robot's planner to ensure that it avoids it at a safe distance. Inflation is performed prior to planning to expand obstacles uniformly in all dimensions by a certain amount (typically the robot's radius, or maximum(length, width) to ensure that the planner avoids obstacles by a safe distance. Standard methods for obstacle inflation include performing the Minkowski sum [cite](#) between the robot's radius and the obstacle, cost propagation from the obstacle, dilating obstacles using convolutions, etc. on a grid map. With these preliminaries, we state our problem formulation as follows:

**Formulation III.1.** *To construct an  $n \times n \times m$  grid map representation  $I_{ML}^t$  of obstacles from points  $\mathbf{p} = \{x, y, z, int\}$  and classify each grid  $(r, c) \in I_{ML}^t$  as a true positive (TP), false positive (FP), false negative (FN) obstacle, or true negative (TN) free space and enlarge TP and FN obstacles adaptively based on the robot's preferred velocity direction.*

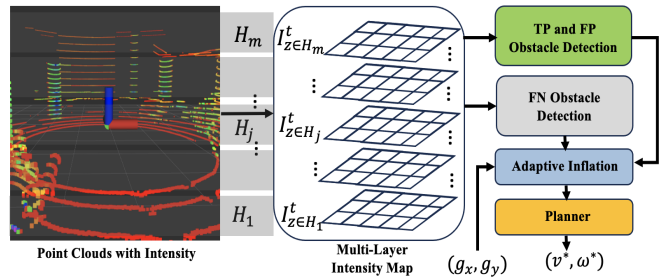


Fig. 2: Our approach's overall system architecture. At time instant  $t$ , the intensities of reflected point clouds from a height interval  $H_j$  (grey rectangles) are used to construct a 2D grid map layer  $I_{z \in H_j}^t$  according to equation 1. Several of such layers are stacked to form a multi-layer intensity map. Some of these layers can be used to detect TP, FP, and FN obstacles. The adaptive inflation enlarges the truly solid (TP, FN) obstacles that the robot must avoid in the direction opposite to the robot's goal  $(g_x, g_y)$  direction, and ignores passable obstacles (FP). The planner finally uses the inflated map to compute collision-free linear and angular velocities  $v^*, \omega^*$ .

## IV. OUR APPROACH

In this section, we discuss how 3D point cloud intensities can be used to construct the multiple 2D grid map layers of a multi-layer intensity map. The input point clouds could be obtained from any sensor such as a 3D lidar or a depth camera that also measures the intensity of the points reflected from surrounding objects. We show how different layers of the intensity map can be used to accurately differentiate solid obstacles from passable objects, and identify transparent obstacles. Finally, we detail our obstacle inflation strategy, which enables robots to navigate through passable obstacles, and narrow passages.

### A. Multi-Layer Intensity Map

We construct a single layer of the intensity map at any time instant  $t$  as follows,

$$I_{z \in H_j}^t(r, c) = \frac{\sum_x \sum_y int}{g^2} \quad (1)$$

$$\forall x \in [x_{low}, x_{low} + g], y \in [y_{low}, y_{low} + g],$$

$$x_{low} = \left\lfloor \left(r - \frac{n}{2}\right) \cdot g \right\rfloor \text{ and } y_{low} = \left\lfloor \left(c - \frac{n}{2}\right) \cdot g \right\rfloor$$

$$H_j = [low_j, high_j], low_j \leq high_j,$$

where  $low_j$ , and  $high_j$  are the limits for all the points whose intensities must be considered for the map along the  $z$  direction. Extending this definition, we construct a *multi-layer* intensity map as a stacking of  $m$  layers as,

$$I_{ML}^t(r, c) = [I_{z \in H_1}^t \mid I_{z \in H_2}^t \mid \dots \mid I_{z \in H_m}^t], \quad (2)$$

where  $H_1, H_2, \dots, H_m$  are non-overlapping intervals of  $z$  limits.  $(r, c)$  is omitted on the right for readability.

We choose stack multiple non-overlapping layers at various heights instead of combining the points' intensities at all heights into a unified layer. This is due to the flexibility that multiple layers provide in analyzing and modifying them

individually. Furthermore, individual layers can be combined after modification and used for planning the robot's trajectories. We highlight these benefits in the following sections.

### B. Obstacle Detection

In this section, we describe how challenging obstacles such as tall grass, string/beaded curtains (false positives), and transparent objects (false negatives) can be detected using our multi-layer intensity map.

#### 1) Differentiating True and False Positive Obstacles:

Existing methods that use various sensor modalities typically detect many thin, pliable obstacles such as tall grass, and passable objects such as string/beaded curtains as solid obstacles that must be avoided. During navigation, such inaccurate detections cause the robot to freeze or oscillate perpetually without reaching its goal. We demonstrate how such false positive obstacles can be detected using the multi-layer intensity map.

Let us consider three layers  $I_{z=0}^t, I_{z \in (0,h]}^t, I_{z \in [-h,0)}^t$  of the intensity map. If a grid location  $(r, c)$  belonging to all three layers satisfies the following condition  $\mathcal{C}$ , we classify that grid as a false positive obstacle:

$$\mathcal{C}(r, c) : I_{z=0}^t(r, c), I_{z \in (0,h]}^t(r, c), I_{z \in [-h,0)}^t(r, c) \leq \Gamma. \quad (3)$$

Here,  $\Gamma$  is an intensity threshold. Using this condition, we construct TP and FP intensity maps for planning as,

$$I_{TP}^t(r, c) = \max(I_{z=0}^t(), I_{z \in (0,h]}^t(), I_{z \in [-h,0)}^t()) \quad \forall \text{ grid} \mid \mathcal{C}(r, c) \text{ is False} \quad (4)$$

$$I_{FP}^t(r, c) = \max(I_{z=0}^t(), I_{z \in (0,h]}^t(), I_{z \in [-h,0)}^t()) \quad \forall \text{ grid} \mid \mathcal{C}(r, c) \text{ is True} \quad (5)$$

2) *Detecting False Negative Obstacles:* False negative obstacles are typically transparent objects that allow most of the laser rays from a sensor to pass through. However, a small neighborhood of points with low intensities are detected for laser rays that are incident  $\sim 0^\circ$  on a transparent surface only along the  $z = 0$  plane. Our approach extrapolates this small neighborhood to detect solid transparent obstacles.

Consider two layers  $I_{z=0}^t$  and  $I_{z=-\epsilon}^t$  in the multi-layer intensity map at time instant  $t$ . Here,  $\epsilon$  is a small positive value. To isolate the low-intensity neighborhood of points reflected from the transparent object, we first calculate  $I_{z=0}^t \ominus I_{z=-\epsilon}^t$ . This removes all the points reflected from the same obstacles in both the layers and retains only the points corresponding to the small glass neighborhood. To indicate the presence of transparent obstacles for subsequent time steps, we transform  $I_{z=0}^t \ominus I_{z=-\epsilon}^t$  based on the robot's motion as,

$$I_{FN}^t = T \cdot (I_{z=0}^t \ominus I_{z=-\epsilon}^t), \quad (6)$$

where  $T$  is a  $4 \times 4$  transformation matrix whose rotational component is based on the robot's yaw, the translational component is based on its motion from time  $t$  to  $t + 1$ . Finally, we augment subsequent time's  $I_{FN}^{t+1}$  using  $I_{FN}^t$  as,

$$I_{FN}^{t+1} = I_{FN}^{t+1} \cup I_{FN}^t. \quad (7)$$

### C. Adaptive Obstacle Inflation

In narrow and dense scenarios, uniformly inflating obstacles (as explained in section III-D) could close the available free space leading to the robot freezing problem [40], where the robot perpetually halts or oscillates without reaching its goal. If obstacles are not inflated, the robot could move close to the obstacles and even collide with them. Additionally, false positive obstacles that can be traversed need not be inflated. Therefore, our approach adaptively inflates the obstacles based on the robot's goal direction. Obstacles are majorly inflated in the direction opposite to the robot's goal/preferred direction, and minorly inflated in all other directions. This ensures that the robot does not navigate too close to a solid obstacle, while also never closing free space near narrow passages.

Our inflation is performed using the convolution operation on obstacles by computing the appropriate kernel matrices  $K$  of size  $e \times e$  as follows. Let  $(g_x, g_y)$  be the goal location relative to the robot's coordinate frame. The goal direction can be defined by the slope  $\tan \frac{g_y}{g_x}$ . To design a kernel matrix  $K$  to inflate obstacles in the opposite direction, we first find the line perpendicular to the goal direction relative to the kernel, passing through its center  $(\frac{e}{2}, \frac{e}{2})$  as,

$$f(r^K, c^K) = c^K + \frac{1}{\tan(g_y/g_x)} \cdot r^K + \text{const} \quad (8)$$

$$\text{const} = -\left(\frac{e}{2} + \frac{e}{2 \cdot \tan(g_y/g_x)}\right).$$

Here,  $(r^K, c^K)$  represent the row and column on the kernel. Next, the kernel can be constructed as,

$$K(r^K, c^K) = \begin{cases} 0 & \forall \{r^K, c^K \mid f(r^K, c^K) > 0\} \\ 1 & \text{Otherwise.} \end{cases} \quad (9)$$

Finally, using  $K$ , we convolve our multi-layer intensity map as,

$$I_{in\,flate}^t = (I_{TP}^t \cup I_{FN}^t) \otimes K. \quad (10)$$

$I_{in\,flate}^t$  contains inflated True Positive and False Negative obstacles. To add information about false positive obstacles prior to planning, we perform,

$$I_{plan}^t = I_{in\,flate}^t \cup I_{FP}^t. \quad (11)$$

### D. Planning

The final planning intensity map  $I_{plan}^t$  can be used with any motion planner to evaluate a candidate linear and angular velocity's  $(v, \omega)$  obstacle or collision cost. This can be done by extrapolating the trajectory produced by  $(v, \omega)$  relative to  $I_{plan}^t$  as in [34], [16] as,

$$\begin{aligned}
\text{Traj}^{I_{plan}^t} &= [(r_1, c_1), \dots, (r_j, c_j), \dots, (r_p, c_p)] \\
\text{Obstacle Cost} &= \sum_{j=1}^p I_{plan}^t(r_j, c_j).
\end{aligned} \tag{12}$$

## V. RESULTS AND ANALYSIS

In this section, we summarize our method’s implementation details and evaluation metrics. Then, we present the details of the experiments conducted to highlight the benefits of our approach.

### A. Implementation

We use a Boston Dynamics Spot robot for outdoor experiments and a Turtlebot 2 robot for indoor experiments. The Spot robot is equipped with an Intel NUC 11 (a mini-PC with Intel i7 CPU and NVIDIA RTX 2060 GPU) and a Velodyne VLP16 LiDAR. The Turtlebot is equipped with a laptop (with an Intel i9 CPU and an Nvidia RTX 2080 GPU) and a Velodyne VLP16 LiDAR. We particularly use Velodyne LiDAR’s *dual return mode* since it captures the details of complex environments that contain scattered small objects and non-opaque surfaces such as glass [41].

### B. Evaluation Metrics

We use the following metrics to compare our method’s navigation performance with VERN [16] (Outdoor), Spot’s inbuilt autonomy (Outdoor), GA-Nav [14] (Outdoor), Detecting glass in SLAM [42], UCTNet [13], DWA with laser scan [10], and DWA with Occupancy Map [12].

VERN is a vegetation-aware navigation approach that uses a vision-based vegetation classifier and a set of LiDAR occupancy maps for perception. Spot’s in-built autonomy incorporates a set of stereo cameras around the robot to estimate the obstacles and ground plane to navigate to a goal. DWA is a local planner that uses a 2D LiDAR scan or an occupancy map to perform obstacle avoidance. GA-Nav combines semantic segmentation for terrain navigability estimation with a LiDAR-based elevation map for outdoor navigation. Detecting glass in SLAM [42] uses the specular reflection of laser beams from the glass to map environments that include glass. UCTNet [13] is a semantic segmentation method that uses RGBD data to segment indoor scenes based on available objects such as curtains, doors, mirrors, etc.

**Success Rate** - Number of successful goal-reaching attempts (without collisions with solid objects or freezing) out of the total number of trials.

**Normalize Traj. Length** - The ratio between the robot’s trajectory length and the straight-line goal distance.

**F-Score** - A measure of object detection accuracy of the intensity map calculated as a weighted average of the precision and recall. Values are between 0 and 1, where 1 indicates the best accuracy and 0 denotes the worst.

Scenario	Method	Success Rate (%)	Norm. Traj. Length	F-Score
Scn. 1	DWA with laser scan [10]	0	0.342	0.119
	DWA with occupancy map [12]	0	0.411	0.198
	Detecting glass in SLAM [42]	70	0.895	0.764
	UCTNet [13]	50	0.633	0.487
	Ours	<b>80</b>	<b>1.052</b>	<b>0.82</b>
Scn. 2	DWA with laser scan [10]	0	1.865	0.169
	DWA with occupancy map [12]	0	1.994	0.156
	Detecting glass in SLAM [42]	0	2.163	0.463
	UCTNet [13]	20	0.725	0.645
	Ours	<b>70</b>	<b>1.241</b>	<b>0.791</b>
Scn. 3	DWA with laser scan [10]	20	1.571	0.451
	DWA with occupancy map [12]	20	1.482	0.429
	Spot’s Inbuilt Autonomy	10	0.311	0.378
	GA-Nav [14]	40	0.576	0.552
	VERN [16]	70	1.154	0.753
Ours	<b>80</b>	<b>1.106</b>	<b>0.844</b>	
Scn. 4	DWA with laser scan [10]	0	1.543	0.372
	DWA with occupancy map [12]	0	1.412	0.359
	Spot’s Inbuilt Autonomy	0	0.298	0.307
	GA-Nav [14]	10	0.587	0.456
	VERN [16]	50	1.267	0.677
Ours	<b>70</b>	<b>1.146</b>	<b>0.735</b>	

TABLE I: Relative performance of our method versus other methods on various metrics.

### C. Testing Scenarios

- **Scenario 1** - Indoor scenario with glass and concrete walls and dynamic humans.
- **Scenario 2** - Indoor scenario with a narrow passage covered with a beaded/string curtain.
- **Scenario 3** - Outdoor scenario with tall grass, bushes, and trees separated from each other.
- **Scenario 4** - Outdoor scenario with tall grass, bushes, and trees closely intertwined with each other.

### D. Analysis and Comparison

We present the qualitative navigation experiment results for the four scenarios in Fig. 3 and the quantitative results in Table I. Scenarios 1 and 2 are complex indoor settings, whereas Scenarios 3 and 4 are outdoor settings. We observe that our method demonstrate the highest success rate compared to the other methods in all four scenarios.

In Scenario 1, 2D laser scan-based and occupancy map-based DWA planners fail to identify the glass region since they do not incorporate LiDAR intensity for object detection. UCTNet based indoor segmentation fails to identify the glass region from RGB-D inputs consistently. Hence, these methods lead to collisions with the glass by assuming the region is passable. The detecting glass in SLAM can identify the glass region using LiDAR intensity and avoid it. However, our method’s multi-layer map formulation leads to consistent glass detection which results in a higher F-score compared to the other methods.

Scenario 2 includes a passable string curtain which is detected as an obstacle from the 2D laser scan and occupancy map based DWA methods. Hence, these three methods attempt to avoid the curtain and collide with the glass during navigation. Further, the glass detection SLAM method identifies both the curtain and the glass as obstacles. Hence, all three methods demonstrate poor success rates in scenario 2. UCTNet can identify the curtain in certain instances based on the camera viewpoint and lighting condition. However, its inconsistent segmentation results in collisions. In con-

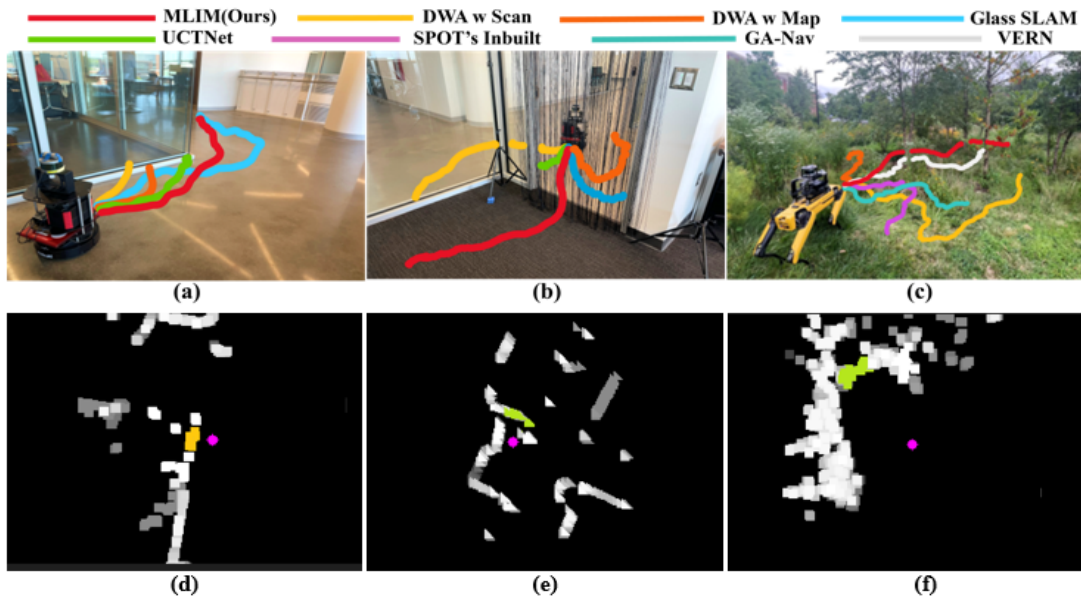


Fig. 3: Robot trajectories when navigating in different complex indoor and outdoor environments using: Intensity maps (ours); DWA with laser scan [10]; DWA with occupancy map [12]; Detecting glass in SLAM [42]; UCTNet [13]; Spot’s Inbuilt Autonomy; and VERN [16]. In indoor scenarios, we observe that intensity maps identifies transparent objects such as glass as obstacles to avoid and objects such as string curtains as passable for navigation. In outdoor scenarios, intensity maps can identify solid objects such as trees even when they are hidden behind navigable vegetation such as tall grass.

trast, our method demonstrates a significantly high success rate irrespective of the lighting conditions due to the  $360^\circ$  LiDAR-based intensity map formulation.

Scenarios 3 and 4 includes traversable tall grass and non-traversable bushes and trees. However, the two DWA methods identify all such vegetation regions as obstacles due to 2D laser scan-based obstacle detection. Hence, such a method leads to freezing and longer detours during navigation. Similarly, Spot’s inbuilt autonomy struggles to estimate the ground and free space from its vision-based perception in both Scenario 3 and Scenario 4. Hence, the robot demonstrates highly unstable motion in vegetation. In Scenario 3, VERN is able to navigate through tall grass while avoiding trees and bushes using its vision-based classifier and the occupancy map formulation. However, VERN’s vision-based classifier could not detect trees behind the grass region in Scenario 4 since they are closely intertwined. In contrast, our method’s multi-layer intensity map representation identifies such hidden solid objects to avoid during navigation. Hence, our method demonstrates a relatively higher success rate and F-core in Scenario 4.

**Benefits of Adaptive Inflation:** We use Scenarios 2 and 3, which include narrow passages to highlight the benefits of our adaptive inflation formulation. Laserscan and occupancy map-based DWA methods use uniform inflation around the obstacles to avoid collisions when navigating close to the obstacles. However, such inflation could close the narrow passages and represent them as obstacle regions. This results in robot freezing or longer trajectories in the presence of narrow free spaces between the obstacles. However, our adaptive inflation preserves the narrow free spaces in the

cost map while inflating the obstacles to minimize the risk of collisions. Hence, our method can navigate through narrow spaces (e.g., through a small door in Scenario 2 and between the trees in Scenario 3) and reach the goals using a significantly shorter trajectory.

## VI. CONCLUSIONS, LIMITATIONS AND FUTURE WORK

We introduce a novel obstacle representation designed to enhance autonomous robot navigation in complex indoor and outdoor environments. Based on the intensity of reflected points from point clouds, intensity maps effectively characterizes obstacles by their height, solidity, and opacity. Also, we present an adaptive inflation technique that further refines navigation planning by considering obstacle solidity and available free space. We demonstrate significant improvements in navigation metrics such as success rates, trajectory lengths, and F-scores, validating our proposed approach.

Our method has a few limitations. Since our multi-layer map representation is based on point cloud intensity, it cannot identify passable objects such as cloth curtains and metal fences. This is especially important because the navigability of such objects depends on the context (e.g., window curtain may not be passable but door curtains are generally passable). Hence, semantic understanding of the environment is required for such cases. Further, our method cannot detect extremely thin objects such as thin poles since 3D point cloud may not capture them.

## REFERENCES

- [1] L. Zhang, Z. Chen, W. Cui, B. Li, C. Chen, Z. Cao, and K. Gao, “Wifi-based indoor robot positioning using deep fuzzy forests,” *IEEE Internet of Things Journal*, vol. 7, no. 11, pp. 10773–10781, 2020.

- [2] N. Ramdani, A. Panayides, M. Karamousadakis, M. Mellado, R. Lopez, C. Christophorou, M. Rebiai, M. Blouin, E. Vellidou, and D. Koutsouris, "A safe, efficient and integrated indoor robotic fleet for logistic applications in healthcare and commercial spaces: the endorse concept," in *2019 20th IEEE International Conference on Mobile Data Management (MDM)*. IEEE, 2019, pp. 425–430.
- [3] D. Conte, S. Leamy, and T. Furukawa, "Design and map-based teleoperation of a robot for disinfection of covid-19 in complex indoor environments," in *2020 IEEE international symposium on safety, security, and rescue robotics (SSRR)*. IEEE, 2020, pp. 276–282.
- [4] R. R. Shamshiri, C. Weltzien, I. A. Hameed, I. J. Yule, T. E. Grift, S. K. Balasundram, L. Pitonakova, D. Ahmad, and G. Chowdhary, "Research and development in agricultural robotics: A perspective of digital farming," 2018.
- [5] J. Champ, A. Mora-Fallas, H. Goëau, E. Mata-Montero, P. Bonnet, and A. Joly, "Instance segmentation for the fine detection of crop and weed plants by precision agricultural robots," *Applications in plant sciences*, vol. 8, no. 7, p. e11373, 2020.
- [6] M. S. Couceiro, D. Portugal, J. F. Ferreira, and R. P. Rocha, "Sem-fire: Towards a new generation of forestry maintenance multi-robot systems," in *2019 IEEE/SICE International Symposium on System Integration (SII)*. IEEE, 2019, pp. 270–276.
- [7] H. Mei, X. Yang, Y. Wang, Y. Liu, S. He, Q. Zhang, X. Wei, and R. W. Lau, "Don't hit me! glass detection in real-world scenes," in *Proceedings of the IEEE/CVF Conference on Computer Vision and Pattern Recognition*, 2020, pp. 3687–3696.
- [8] M. Kuribayashi, S. Kayukawa, J. Vongkulbhisal, C. Asakawa, D. Sato, H. Takagi, and S. Morishima, "Corridor-walker: Mobile indoor walking assistance for blind people to avoid obstacles and recognize intersections," *Proceedings of the ACM on Human-Computer Interaction*, vol. 6, no. MHCI, pp. 1–22, 2022.
- [9] M. Hua, Y. Nan, and S. Lian, "Small obstacle avoidance based on rgb-d semantic segmentation," in *Proceedings of the IEEE/CVF international conference on computer vision workshops*, 2019, pp. 0–0.
- [10] D. Fox, W. Burgard, and S. Thrun, "The dynamic window approach to collision avoidance," *IEEE Robotics & Automation Magazine*, vol. 4, no. 1, pp. 23–33, 1997.
- [11] Y. Wu, Y. Wang, S. Zhang, and H. Ogai, "Deep 3d object detection networks using lidar data: A review," *IEEE Sensors Journal*, vol. 21, no. 2, pp. 1152–1171, 2020.
- [12] B. P. Gerkey and K. Konolige, "Planning and control in unstructured terrain," in *ICRA workshop on path planning on costmaps*. Citeseer, 2008.
- [13] X. Ying and M. C. Chuah, "Ucnet: Uncertainty-aware cross-modal transformer network for indoor rgb-d semantic segmentation," in *European Conference on Computer Vision*. Springer, 2022, pp. 20–37.
- [14] T. Guan, D. Kothandaraman, R. Chandra, A. J. Sathiamoorthy, K. Weerakoon, and D. Manocha, "Ga-nav: Efficient terrain segmentation for robot navigation in unstructured outdoor environments," *IEEE Robotics and Automation Letters*, vol. 7, no. 3, pp. 8138–8145, 2022.
- [15] T. M. Petty, J. D. Fernandez, J. N. Fischell, and L. A. De Jesús-Díaz, "Lidar attenuation through a physical model of grass-like vegetation," *Journal of Autonomous Vehicles and Systems*, vol. 2, no. 2, p. 021003, 2022.
- [16] A. Jagan Sathiamoorthy, K. Weerakoon, T. Guan, M. Russell, D. Conover, J. Pusey, and D. Manocha, "Vern: Vegetation-aware robot navigation in dense unstructured outdoor environments," *arXiv e-prints*, pp. arXiv-2303, 2023.
- [17] L. Di Giammarino, I. Aloise, C. Stachniss, and G. Grisetti, "Visual place recognition using lidar intensity information," in *2021 IEEE/RSJ International Conference on Intelligent Robots and Systems (IROS)*. IEEE, 2021, pp. 4382–4389.
- [18] K. Sullivan, W. Lawson, and D. Sofge, "Fusing laser reflectance and image data for terrain classification for small autonomous robots," in *2014 13th International Conference on Control Automation Robotics & Vision (ICARCV)*. IEEE, 2014, pp. 1656–1661.
- [19] S. Laible, Y. N. Khan, K. Bohlmann, and A. Zell, "3d lidar-and camera-based terrain classification under different lighting conditions," in *Autonomous Mobile Systems 2012: 22. Fachgespräch Stuttgart, 26. bis 28. September 2012*. Springer, 2012, pp. 21–29.
- [20] C. Reymann and S. Lacroix, "Improving lidar point cloud classification using intensities and multiple echoes," in *2015 IEEE/RSJ International Conference on Intelligent Robots and Systems (IROS)*. IEEE, 2015, pp. 5122–5128.
- [21] J. Guo, P. V. Borges, C. Park, and A. Gawel, "Local descriptor for robust place recognition using lidar intensity," *IEEE Robotics and Automation Letters*, vol. 4, no. 2, pp. 1470–1477, 2019.
- [22] M. Aldibaja, N. Suganuma, R. Yanase, and K. Yoneda, "Reliable graph-slam framework to generate 2d lidar intensity maps for autonomous vehicles," in *2020 IEEE 91st Vehicular Technology Conference (VTC2020-Spring)*, 2020, pp. 1–6.
- [23] C. Wei, T. Wu, and H. Fu, "Estimating initial guess of localization by line matching in lidar intensity maps," in *Information Technology and Intelligent Transportation Systems: Volume 1, Proceedings of the 2015 International Conference on Information Technology and Intelligent Transportation Systems ITITS 2015, held December 12-13, 2015, Xi'an China*. Springer, 2017, pp. 577–588.
- [24] I. A. Bârsan, S. Wang, A. Pokrovsky, and R. Urtasun, "Learning to localize using a lidar intensity map," 2020.
- [25] T. D. Barfoot, C. McManus, S. Anderson, H. Dong, E. Beerepoot, C. H. Tong, P. Furgale, J. D. Gammell, and J. Enright, "Into darkness: Visual navigation based on a lidar-intensity-image pipeline," in *Robotics Research: The 16th International Symposium ISRR*. Springer, 2016, pp. 487–504.
- [26] Y. H. Shin and D.-C. Lee, "True orthoimage generation using airborne lidar data with generative adversarial network-based deep learning model," *Journal of Sensors*, vol. 2021, pp. 1–25, 2021.
- [27] F. Garestier, P. Bretel, O. Monfort, F. Levoy, and E. Poullain, "Anisotropic surface detection over coastal environment using near-lidar intensity maps," *IEEE Journal of Selected Topics in Applied Earth Observations and Remote Sensing*, vol. 8, no. 2, pp. 727–739, 2014.
- [28] J. Dupeyroux, S. Viollet, and J. R. Serres, "An ant-inspired celestial compass applied to autonomous outdoor robot navigation," *Robotics and Autonomous Systems*, vol. 117, pp. 40–56, 2019.
- [29] J. Li, H. Qin, J. Wang, and J. Li, "Openstreetmap-based autonomous navigation for the four wheel-legged robot via 3d-lidar and ccd camera," *IEEE Transactions on Industrial Electronics*, vol. 69, no. 3, pp. 2708–2717, 2021.
- [30] G. Huskić, S. Buck, and A. Zell, "Gerona: generic robot navigation: a modular framework for robot navigation and control," *Journal of Intelligent & Robotic Systems*, vol. 95, no. 2, pp. 419–442, 2019.
- [31] K. Weerakoon, A. J. Sathiamoorthy, J. Liang, T. Guan, U. Patel, and D. Manocha, "Graspe: Graph based multimodal fusion for robot navigation in unstructured outdoor environments," *arXiv preprint arXiv:2209.05722*, 2022.
- [32] K. M. Wurm, R. Kümmerle, C. Stachniss, and W. Burgard, "Improving robot navigation in structured outdoor environments by identifying vegetation from laser data," in *2009 IEEE/RSJ International Conference on Intelligent Robots and Systems*. IEEE, 2009, pp. 1217–1222.
- [33] K. Weerakoon, A. J. Sathiamoorthy, U. Patel, and D. Manocha, "Terp: Reliable planning in uneven outdoor environments using deep reinforcement learning," in *2022 International Conference on Robotics and Automation (ICRA)*. IEEE, 2022, pp. 9447–9453.
- [34] A. J. Sathiamoorthy, K. Weerakoon, T. Guan, J. Liang, and D. Manocha, "Terrapn: Unstructured terrain navigation using online self-supervised learning," in *2022 IEEE/RSJ International Conference on Intelligent Robots and Systems (IROS)*, 2022, pp. 7197–7204.
- [35] T. Miki, J. Lee, J. Hwangbo, L. Wellhausen, V. Koltun, and M. Hutter, "Learning robust perceptive locomotion for quadrupedal robots in the wild," *Science Robotics*, vol. 7, no. 62, p. eabk2822, 2022. [Online]. Available: <https://www.science.org/doi/abs/10.1126/scirobotics.abk2822>
- [36] T. Homberger, L. Wellhausen, P. Fankhauser, and M. Hutter, "Support surface estimation for legged robots," in *2019 International Conference on Robotics and Automation (ICRA)*. IEEE, 2019, pp. 8470–8476.
- [37] M. Elnoor, A. J. Sathiamoorthy, K. Weerakoon, and D. Manocha, "Pronav: Proprioceptive traversability estimation for legged robot navigation in outdoor environments," 2023.
- [38] G. Kahn, P. Abbeel, and S. Levine, "Badgr: An autonomous self-supervised learning-based navigation system," *IEEE Robotics and Automation Letters*, vol. 6, no. 2, pp. 1312–1319, 2021.
- [39] A. Polevoy, C. Knuth, K. M. Popek, and K. D. Katyal, "Complex terrain navigation via model error prediction," in *2022 International Conference on Robotics and Automation (ICRA)*, 2022, pp. 9411–9417.
- [40] A. J. Sathiamoorthy, U. Patel, T. Guan, and D. Manocha, "Frozone:

Freezing-free, pedestrian-friendly navigation in human crowds,” *IEEE Robotics and Automation Letters*, vol. 5, no. 3, pp. 4352–4359, 2020.

- [41] L. Weerakoon, G. S. Herr, J. Blunt, M. Yu, and N. Chopra, “Cartographer\_glass: 2d graph slam framework using lidar for glass environments,” *arXiv preprint arXiv:2212.08633*, 2022.
- [42] X. Wang and J. Wang, “Detecting glass in simultaneous localisation and mapping,” *Robotics and Autonomous Systems*, vol. 88, pp. 97–103, 2017. [Online]. Available: <https://www.sciencedirect.com/science/article/pii/S0921889015302670>